Synthesis and identification of defective metal-organic frameworks based on chromium and investigation of their catalytic application in the carbon dioxide fixation reaction

Pooneh Pishkar [1], Pouya Pishkar [2]
[1] Department of Chemistry, Faculty of Sciences, Tarbiat Modares University, P.O. Box 14117-13116, Tehran, Islamic Republic of Iran
[2] School of Metallurgy and Materials Engineering, College of Engineering, University of Tehran, Tehran, Iran

ABSTRACT

This research focuses on the synthesis, characterization, and catalytic evaluation of defect-engineered chromium-based MOFs, specifically MIL-101-Cr. Defects were introduced into the structure using benzoic acid as a modulator throughout the solvothermal synthesis method. The study explores the impact of these structural modifications on the catalytic efficiency of MIL-101-Cr in CO_2 fixation reactions. Comprehensive characterization techniques, including XRD, SEM, BET, FTIR, and TPD, were utilized to analyze the structural, morphological, and thermal properties of the defective MOFs. Catalytic tests revealed significant improvements in CO_2 conversion and epoxide ring-opening reactions, with the defective MOFs achieving a conversion rate of up to 90% under optimized conditions. These findings emphasize the promise of defect-engineered MIL-101-Cr as a highly efficient catalyst for sustainable CO_2 utilization, contributing to advancements in green chemistry and environmental remediation.

Keywords: **Metal-organic framework, CO_2 fixation, MIL-101-Cr, Structural defect, Catalysis**

1. *INTRODUCTION*

Metal-organic frameworks (MOFs) have become a flexible category of materials characterized by their exceptional properties, such as high surface area [1], tunable porosity [2], and chemical stability [3]. These properties have positioned MOFs as potential options for diverse uses, including gas storage, separation [4,5], and catalysis [6]. Among the numerous MOFs, chromium-based frameworks have attracted considerable interest because of their structural robustness and catalytic efficiency [7,8]. Notably, MIL-101-Cr is among the most extensively researched chromium-based MOFs, renowned for its exceptional stability and possibility in catalytic and adsorption processes [9,10].

Defect engineering in MOFs has recently become a focal point of research, as the deliberate introduction of defects can significantly enhance material properties [11]. These defects, created through linker modification [12], partial metal substitution [13], or thermal treatment [14], can improve catalytic activity [15], adsorption efficiency [16], and selectivity [17]. Defective MOFs, therefore, present an exciting avenue for tailoring materials to specific applications.

One critical global challenge is the mitigation of carbon dioxide (CO_2) emissions, that play a role in climate change and environmental degradation [18,19]. Carbon dioxide fixation, a process that converts CO_2 into valuable chemicals, has gained attention as a sustainable solution [20,21]. MOFs, particularly those with engineered defects, offer unique advantages for CO_2 fixation due to their enhanced adsorption capacities [22] and catalytic properties [23]. Despite significant progress, the application of defective chromium-based MOFs in CO_2 fixation reactions remains underexplored [24,26].

This study aims to address this gap by synthesizing and characterizing defective chromium-based MOFs and evaluating their catalytic performance in the CO_2 fixation reaction. By introducing defects into the framework, we seek to enhance their catalytic activity and optimize their performance. The objectives of this

research include the development of a systematic synthesis method, comprehensive structural characterization, and detailed catalytic analysis of these materials.

In the following sections, the synthesis, characterization, and catalytic evaluation of defective chromium-based MOFs will be presented, providing insights into their potential as effective catalysts for CO_2 fixation and playing a part in the advancement of sustainable solutions for environmental challenges.

2. *Materials and methods*

2.1. *Materials*

All chemicals were of analytical reagent (AR) grade and used as received without further purification. The materials used in this study are as follows: Chromium(III) nitrate nonahydrate ($Cr(NO_3)_3 \cdot 9H_2O$) (Sigma Aldrich, 98%), ethanol (C_2H_5OH) (E. Merck Inc., 99%), methanol (CH_3OH) (E. Merck Inc., 99%), 1,4-benzenedicarboxylic acid (BDC) (Merck, 98%), deionized water (DI) in order to reaction and washing, N,N'-dimethylformamide (DMF) (Fluka Co., 99%), tetrabutylammonium bromide (TBAB) (99%), benzoic acid (Sigma Aldrich, 99%), acetone (C_3H_6O) (Sigma Aldrich, 99.5%), n-octane (Sigma Aldrich, 98%), styrene oxide (Sigma Aldrich, 97%), and glacial acetic acid (CH_3COOH) (Merck, 100%).

2.2. Synthesis of MIL-101-Cr by the Solvothermal Method

0.8 grams of $Cr(NO_3)_3 \cdot 9H_2O$ and 0.328 grams (2 mmol) of benzene dicarboxylic acid (BDC) were mixed. 1.5 mL of 36% acetic acid and 10 mL of water were added to the reaction. Then, the reaction mixture was transferred into the Teflon-lined autoclave, placed in the furnace, and the furnace was programmed with a heating rate of 22°C/hour until it attained 200°C. It was then cooled back to room temperature using the same heating program. To wash the compound, it was first washed three times with DMF and then sonicated in ethanol for 1 hour. For activation of the compound, solvent exchange was initially performed with methanol for 2 hours, and then with acetone for 24 hours. After drying at room temperature, the compound was moved to a vacuum oven at 120°C for 16 hours for activation. The resulting MOF was then collected [27].

2.3. Synthesis of Defective MIL-101-Cr Structure Using Benzoic Acid

1.2 grams of $Cr(NO_3)_3 \cdot 9H_2O$,3 mmol, 0.498 grams (3 mmol) of BDC, and 0.363 grams (3 mmol) of benzoic acid were mixed, and 15 mL of water was introduced into the reaction. The mixture was subsequently placed into a Teflon-lined autoclave, placed in a furnace, and heated at a rate of 22°C/hour until reaching 220°C. Afterward, the reaction mixture was allowed to cool to room temperature following the same cooling program. To purify the resulting compound, it was washed three times with DMF and then sonicated in ethanol for 1 hour.

For activation, the compound underwent solvent exchange with methanol for 2 hours, followed by solvent exchange with acetone for 24 hours. After air-drying at room temperature, the compound was

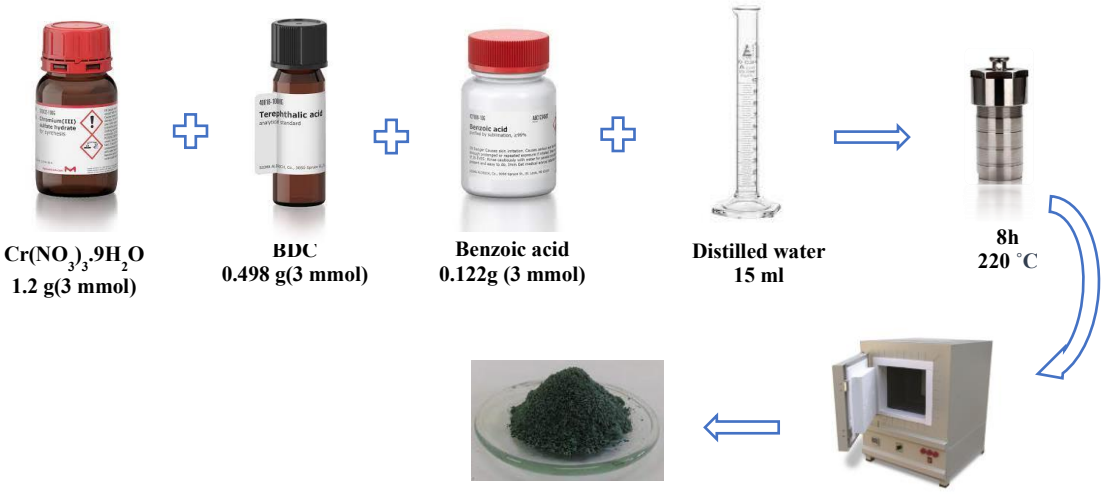

Figure 1- A schematic illustration of synthesis process of defective MIL-101-Cr.

transferred to a vacuum oven at 120∘C for 16 hours for final activation. The obtained MOF was then collected. The synthesis process is illustrated in Figure 1.

3. General Methods for Catalytic CO_2 Fixation Reactions

3.1. General Procedure for Catalytic CO_2 Fixation in Epoxides:

Both synthesized catalysts were evaluated for catalytic CO_2 fixation in epoxides. In a typical reaction, 1–5 mol% catalyst, 10 mmol of epoxide, and 1 mol% TBAB were added to the reactor under 1.5 bar of CO_2 pressure. The reaction temperature was kept constant between 50–110°C. The reaction products were analyzed using FID-GC injection.

3.2. General Procedure for Catalytic Epoxide Ring Opening:

All two synthesized catalysts were tested for catalytic CO_2 fixation in epoxides. In a typical reaction, 1–5 mol% catalyst, 2 mmol of epoxide, and 5 mL of methanol were added to the reactor. The reaction temperature was maintained between 50–110°C. The reaction products were analyzed using FID-GC injection.

3.3. Procedure for CO_2 Cycloaddition Reaction:

The reaction was performed in a glass test tube equipped with a magnetic stirrer. Styrene oxide, the catalyst, and TBAB were added to the test tube. The reaction vessel was purged three times with CO_2 to remove moisture and air, then pressurized with CO_2. Once the test tube reached the desired temperature, the reaction was stirred at 250 rpm.

Following the reaction, the test tube was allowed to cool to ambient temperature, and the excess CO_2 was carefully released. The catalyst was separated via centrifugation, washed three times with methanol, and dried under vacuum at 150°C for 12 hours for reuse.

4. Characterization Techniques

X-ray diffraction (XRD) analysis was carried out using a Siemens 5000d diffractometer, operating at 40 kV, with Kα-Co and Kα-Cu radiation, utilizing the Xpert Philips model. XRD was employed to investigate the crystalline structure and phase purity of the photocatalysts. The structure and surface morphology of the synthesized photocatalysts were analyzed using a scanning electron microscope (SEM, CamScanMV2300), coupled with energy-dispersive X-ray spectroscopy (EDAX, JEOL Centurio spectrometer). This method was used to observe the detailed surface features and elemental composition of the photocatalysts. Fourier transform infrared spectroscopy (FTIR) spectra were recorded with a Rad Bio 7FTS spectrophotometer in KBr pellet form to determine the functional groups present in the material and verify the formation of specific chemical bonds. The surface area of the samples was measured using nitrogen adsorption-desorption isotherms and the Brunauer-Emmett-Teller (BET) method, with a Micromeritics ASAP 2460 instrument. This technique was utilized to assess the surface area and porosity of the photocatalysts, which are critical properties for their catalytic performance. The thermal stability and activation behavior of the sample were evaluated using a thermogravimetric analyzer (TGA, TA SDT650). TGA was used to determine the decomposition temperatures and assess the sample's stability under heat. For the NH_3 and CO_2 adsorption studies, temperature-programmed desorption (TPD) experiments were performed using a NanoSORD NS91 instrument (Sensiran, Iran). This technique was used to examine the adsorption and desorption properties of the catalysts, which are important for understanding their catalytic activity in gas-phase reactions. Additionally, gas chromatography was conducted with a 90A-Ech model to analyze the reaction products and measure the efficiency of the catalysts in catalyzing the desired reactions.

5. Results and Discussion

5.1. powder X-ray diffraction

The powder X-ray diffraction (PXRD) analysis conducted on MIL-101-Cr and its modified counterpart, defective MIL-101-Cr, offers valuable insights into their structural characteristics. Figure 2 illustrates the PXRD patterns of both samples, showing characteristic diffraction peaks at 5.23°, 8.53°, 9.13°, and 16.59°, aligning closely with standard MIL-101-Cr patterns, which validates the successful synthesis and crystallinity of the material [28]. However, It is important to highlight that the defective MIL-101-Cr sample lacks the diffraction peak at approximately 3.37°, which is present in MIL-101-Cr. This absence indicates that the structural modification with BDC may have disrupted certain crystallographic planes in the framework. A comparison of the two samples further highlights differences in peak sharpness and intensity. The sharper and more intense peaks of MIL-101-Cr indicate a higher crystallinity and better structural order, whereas the broader and less pronounced peaks of defective MIL-101-Cr suggest the occurrence of defects caused by BDC. Additionally, the diffraction patterns at lower 2θ values signify the porous nature of the MIL-101-Cr framework [29].

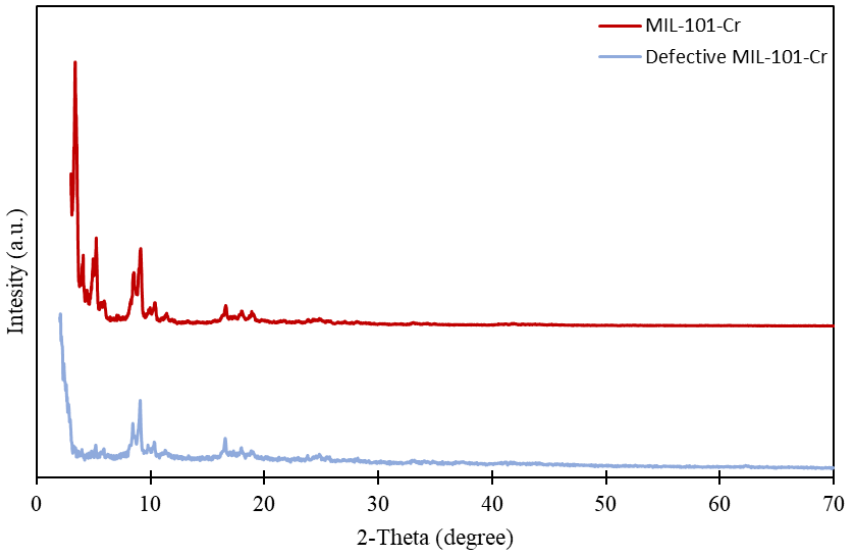

Figure 2- PXRD curves of MIL-101-Cr and defective MIL-101-Cr.

5.2. SEM and energy dispersive x-ray spectroscopy (EDAX)

The SEM analysis of MIL-101-Cr and defective MIL-101-Cr highlights significant differences in their morphological and structural characteristics, shedding light on their potential functionalities. Figure 3 presents the SEM images of MIL-101-Cr and defective MIL-101-Cr captured at different magnifications, providing detailed insights into their structural features. The SEM images of MIL-101-Cr reveal a highly crystalline morphology with uniform octahedral-shaped particles, smooth surfaces, and consistent particle sizes averaging around 150 nm, indicative of the successful synthesis of MIL-101-Cr. The well-defined octahedral shape reflects the high-quality crystallinity and structural integrity of the framework.

In contrast, the SEM images of defective MIL-101-Cr display irregularly shaped particles, ranging from distorted octahedral to amorphous structures, with noticeable surface defects such as cracks and pores caused by the incorporation of benzoic acid. The particle size for defective MIL-101-Cr varies more significantly, ranging between 100 and 200 nm, highlighting the heterogeneity introduced by the defect engineering. The surface irregularities and structural defects in defective MIL-101-Cr are more evident under higher magnification, suggesting potential enhancements in functional properties, including increased specific surface area or improved adsorption and catalytic capabilities [29,31].

This comparison emphasizes that while MIL-101-Cr exhibits pristine and uniform octahedral morphology, the structural irregularities in defective MIL-101-Cr, including its varied shapes and defects, make it a candidate for applications requiring enhanced reactivity or tailored material properties. The differences observed under varying magnifications in Figure 3 offer valuable insights for advanced material design.

The EDAX analysis was performed to determine the elemental compositions of MIL-101-Cr and its defective counterpart. The obtained spectra, as shown in Figure 4, verified the existence of C, O, and Cr as the primary elemental components in both samples. The analysis highlights significant differences in elemental composition due to the introduction of benzoic acid in the defective MIL-101-Cr sample.

In the defective MIL-101-Cr sample, the carbon content was significantly higher (50.70%) compared to the standard MIL-101-Cr sample, that contained 36.25%. This increase in carbon is due to the inclusion of benzoic acid into the structure, introducing additional carbon atoms. Conversely, the oxygen content in the defective sample (46.96%) was notably lower than that in the standard sample (61.14%), indicating a relative decrease in oxygen content due to the structural modifications.

Interestingly, the chromium content remained relatively stable across both samples, ranging between 2.3% and 2.6%. This consistency in chromium levels underscores the stability of this element within the framework, even after defect engineering with benzoic acid. The elemental shifts observed through EDAX analysis emphasize the structural and compositional changes induced by benzoic acid incorporation,

providing valuable insights into the modified material's properties. EDAX's quantitative results of MIL-101-Cr and defective MIL-101-Cr is presented in table 1.

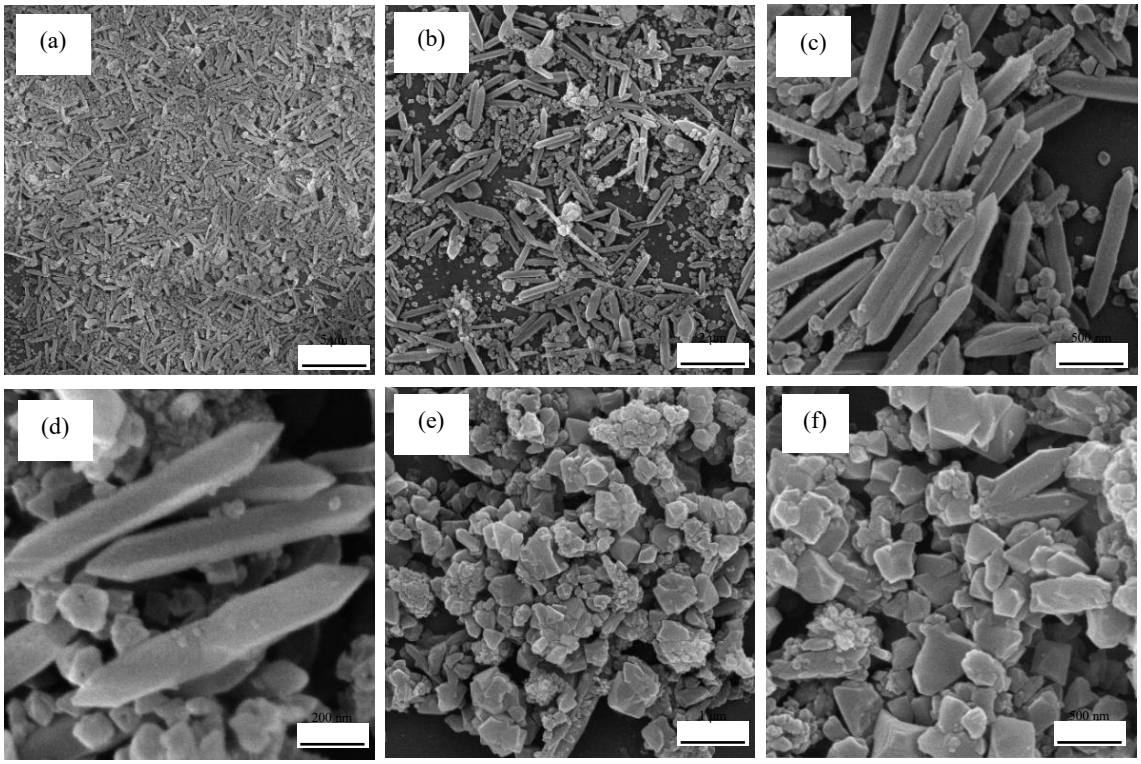

Figure 3- SEM images of (a-d) MIL-101-Cr and (e-f) defective MIL-101-Cr.

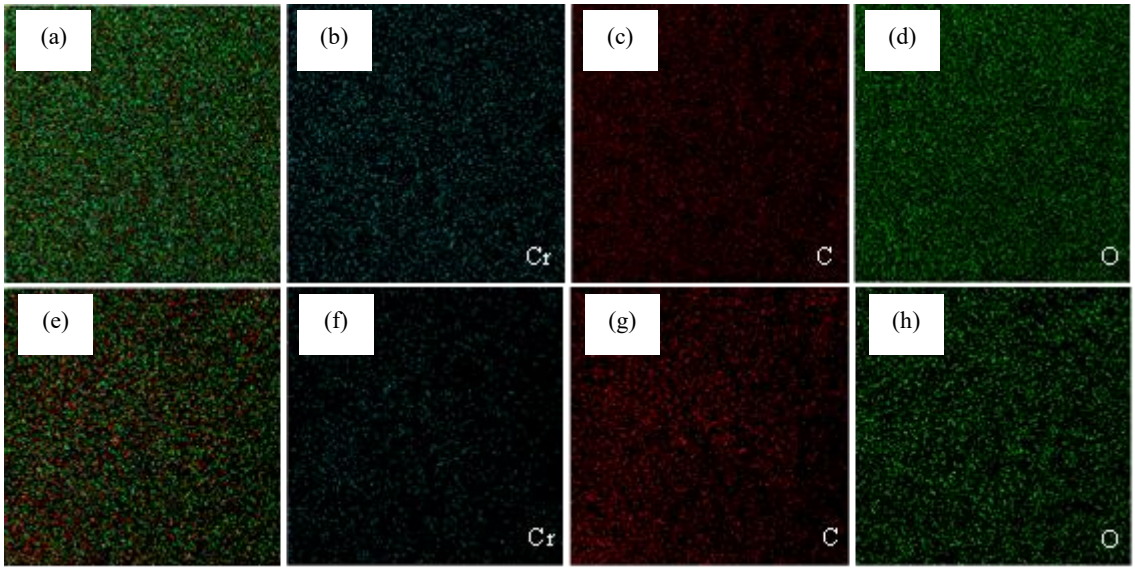

Figure 4- EDAX images of (a-d) MIL-101-Cr and (e-h) defective MIL-101-Cr.

Table 1- EDAX's quantitative results of MIL-101-Cr and defective MIL-101-Cr.

SAMPLE	Element	W%	A%
MIL-101-Cr	C	36.25	43.80
MIL-101-Cr	O	61.14	55.47
MIL-101-Cr	Cr	2.61	0.73

MIL-101-Cr	SUM	100.00	100.00
Defective MIL-101-Cr	C	50.70	58.62
Defective MIL-101-Cr	O	46.96	40.75
Defective MIL-101-Cr	Cr	2.34	0.62
Defective MIL-101-Cr	SUM	100.00	100.00

5.3. FTIR

As indicated by the FTIR spectrum shown in Figure 5a, the peak at 1700 cm^{-1} corresponds to free BDC. The peak at 1508 cm^{-1} is related to C=C, and the peak around 1400 cm^{-1} is attributed to the symmetric stretching vibration of C-O-C. The peak at approximately 570 cm^{-1} is assigned to the Cr-O vibration. Comparing the IR spectrum of the activated sample with the non-activated sample in Figure 5b reveals that, after activation, the peak corresponding to free BDC around 1700 cm^{-1} disappears. This change indicates that the activation method used for this sample was effective [33]. Additionally, the FTIR spectra of defective compound, also depicted in Figure 5c, were analyzed. As observed, these spectra show no differences compared to the FTIR spectrum of MIL-101-Cr, suggesting that the functional groups and chemical structure remain consistent despite the introduction of defects.

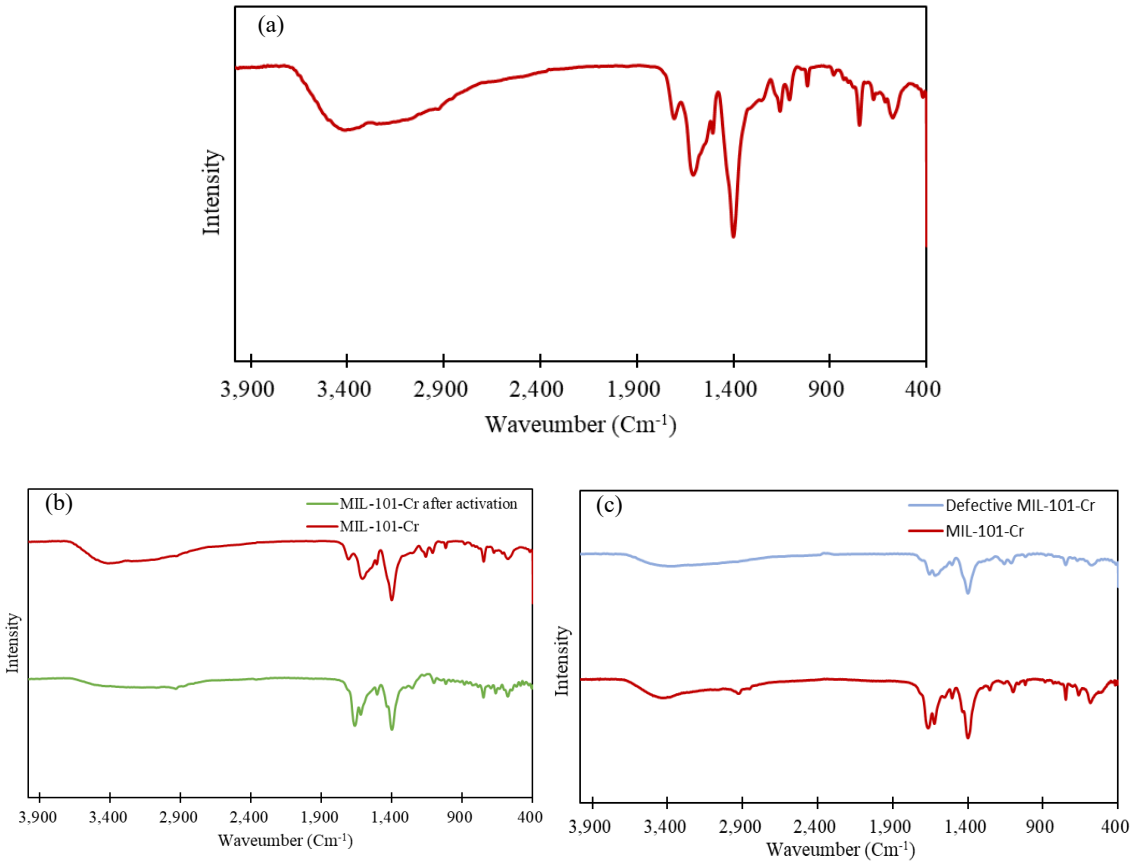

Figure 5- FT-IR plots of (a) MIL-101-Cr, (b) differences in non-activated and activated MIL-101-Cr and (c) differences in non-defective and defective MIL-101-Cr.

5.4. BET

The porosity of these materials was analyzed through nitrogen adsorption at 77 K. The resulting isotherms (shown in Figure 6a) were Type II for the primary MIL-101-Cr sample and Type III for the defective sample modified with benzoic acid. The calculated BET surface area for MIL-101-Cr was 948.91 m^2/g, while for the defective sample, it was significantly reduced to 418.15 m^2/g. This reduction in surface area aligns with the expected loss of linkers in the structure after defect formation.

Additionally, the pore size increased from 31.66 Å in MIL-101-Cr to 45.16 Å in the defective sample, confirming the structural modifications and defect generation. These changes (illustrated in Figure 6b) highlight the impact of benzoic acid on the material's structure, leading to decreased surface area and increased pore volume, which is consistent with the removal of linkers and the creation of defects in the framework [33].

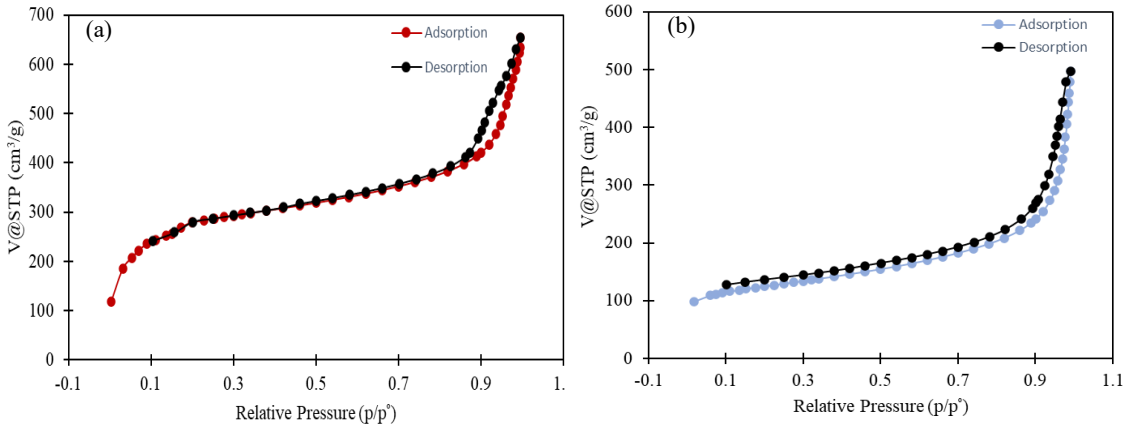

Figure 6-BET plots of (a) MIL-101-Cr and (b) defective MIL-101-Cr.

5.5. NH_3-TPD

Temperature-programmed desorption (TPD) is a method used to measure the adsorption of molecules on the surface of materials by examining the desorption rate as the temperature increases. Adsorbed molecules can be desorbed in a stream of pure carrier gas, allowing the identification of specific characteristics of the materials. For the mentioned samples, qualitative and quantitative analysis of acidic active sites was conducted using NH_3 gas.

As shown in Figure 7a-b, the NH_3-TPD analysis reveals significant differences between the defective and non-defective samples. At a pressure of 1 atmosphere, a heating rate of 1–100°C, and a maximum temperature of 100°C, the defective sample desorbed 0.328 mmol of gas, which is significantly higher than the non-defective structure, which desorbed only 0.017 mmol. This higher desorption in the defective sample indicates the creation of Lewis acid sites within the structure [34]. The N-TPD results of non-defective and defective MIL-101-Cr is presented in table 2.

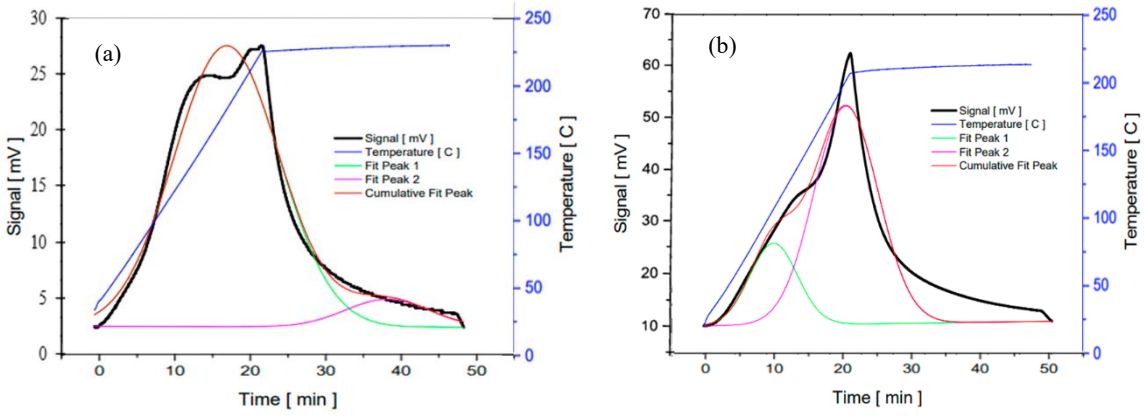

Figure 7- NH_3-TPD graphs of (a) MIL-101-Cr and (b) defective MIL-101-Cr.

Table 2- NH_3-TPD results of (a) MIL-101-Cr and (b) defective MIL-101-Cr.

Sample	Peak #	Area	Height	Temp. (°C)	Time (min)	mmole NH_3	mmole NH_3/g

MIL-101-Cr	1	364.049	20.863	178.918	15.53629	0.0170	0.3830
Defective MIL-101-Cr	1	712.902	35.193	210.817	19.73366	0.0328	0.5436

5.6. TGA

TGA and derivative thermogravimetric (DTGA) evaluations of defective MIL-101-Cr in its activated and non-activated states highlight the transformative effects of activation on the material's thermal performance. Figure 8a-b illustrates the TGA and DTGA curves for both samples, providing a detailed comparison of their thermal behaviors.

In the initial phase (30–100°C), both samples undergo weight reduction, attributed to the release of physically adsorbed water. The activated sample experiences a smaller weight decrease, as shown in Figure 8a, suggesting that the activation process effectively eliminates residual solvents. Between 100–350°C, both materials remain relatively stable, with activated defective MIL-101-Cr demonstrating enhanced thermal endurance due to the removal of OH/F groups and structural refinement [35].

Within the 350–550°C range, the samples exhibit a noticeable weight reduction associated with the decomposition of the organic linker (BDC) and the disintegration of the framework. Figure 8a highlights that this process initiates at lower temperatures for defective MIL-101-Cr (around 350°C) but is delayed in activated defective MIL-101-Cr (starting near 450°C), showcasing the superior structural integrity of the activated form. At 550°C, a stable residue of Cr_2O_3 forms [29].

DTGA analysis, also depicted in Figure 8b, further indicates that activated defective MIL-101-Cr is less prone to weight loss at lower and mid-temperature ranges and demonstrates better resilience against framework collapse. The observed peaks in the DTGA curves suggest the existence of unstable chemical components in defective MIL-101-Cr, while activated defective MIL-101-Cr displays a more robust and optimized structure due to the effective elimination of these unstable groups [36].

In summary, activation significantly enhances the material's thermal properties, slows its degradation, and improves its structural durability under high temperatures, as evidenced by the comparative TGA and DTGA curves in Figure 8, making the activated form more suitable for demanding thermal environments.

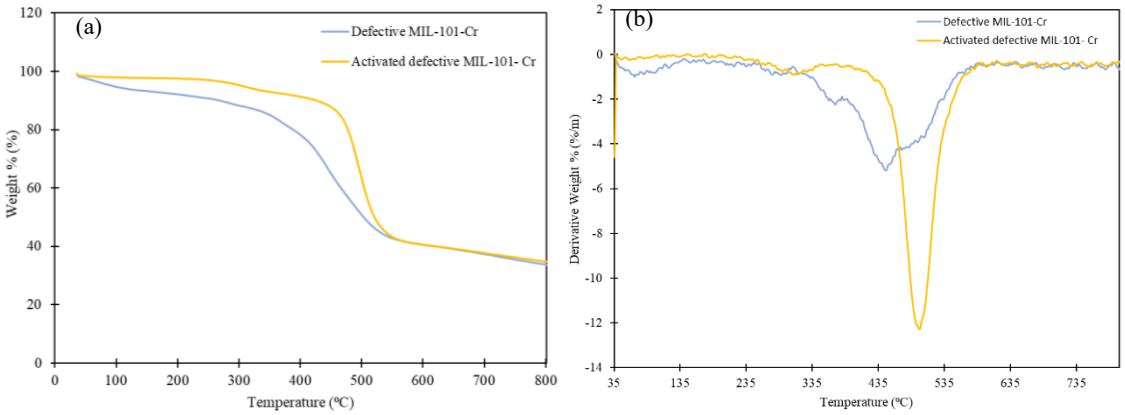

Figure 8- (a) TGA plots and (b) DTG plots of non-defective and defective MIL-101-Cr.

5.7. CO_2 Fixation

The time and amount of different catalysts were tested to determine the optimal values. Table 3 shows the initial tests. As indicated, the conversion rate for the defect-free sample was only 11%. For the sample defective with benzoic acid, the conversion rate reached 38%.

The parameters for the MOF defective with benzoic acid were optimized to achieve maximum conversion and selectivity. Table 3 presents the optimized values. In this experiment, factors such as the amount of co-catalyst, volume of epoxide styrene, amount of defective catalyst, temperature, and reaction time were varied to find the optimal values. Based on the experiments, the optimal reaction time was determined to be 24 hours.

Table 3 highlights the effects of increasing temperature on the cyclization reaction of CO_2. As the temperature increased from 50 to 110°C, both conversion and selectivity showed significant improvement. Additionally, the effects of slightly increasing the amount of co-catalyst on the reaction yield were also evident. Sixty milligrams of benzoic acid- defective MIL-101-Cr exhibited the highest catalytic activity in this reaction. The highlighted parameters in Table 3 represent the optimal values.

Table 3- Initial tests for synthesized compounds

Reaction number	Volume of Styrene Epoxide (ml)	Amount of Catalyst (mg)	Amount of TBABr (g)	Reaction Time	Reaction Temperature (ºC)	Conversion	Selectivity
MIL-101-Cr	1,14	30	0,05	24	50	11%	92%
Defective(banzoic acid)	1,14	7	0,01	24	50	39%	92%
Defective(benzoic acid)	0,25	60	0,1	24	90	76%	88%
Defective(benzoic acid)	0,25	35	0,1	24	90	77%	96%
Defective(benzoic acid)	0,25	30	0,15	24	90	73%	90%
Defective(benzoic acid)	0,25	30	0,1	24	110	86%	88%
Defective(benzoic acid)	0,25	60	0,15	24	110	90%	98%

5.7.1. Investigating the Catalytic Effects of Synthesized MOFs on the Epoxide Styrene Ring-Opening Reaction

The direct nucleophilic attack of the bromide ion on the epoxide group in epoxide styrene leads to the ring-opening of the epoxide and the creation of a bromohydrin intermediate. This reaction initiates during the CO_2 fixation process, with epoxide styrene serving as the primary reactant. The overall reaction mechanism involves the attack of the bromide ion on the carbon atom of the epoxide, breaking the bond between carbon and oxygen. This results in the formation of a three-membered ring containing the bromide ion and an OH alcohol group bound to the carbon atom. Protonation of the OH group by an acidic catalyst forms the final product, bromohydrin [37]. Investigating the epoxide ring-opening reaction provides valuable insight into the efficiency of the CO_2 fixation reaction, as the epoxide ring-opening is an essential step in the CO_2 fixation procedure. Understanding the kinetics of the epoxide ring-opening reaction enables the optimization of the CO_2 fixation process. For instance, temperature, pressure, and catalyst concentration can be optimized. Therefore, this reaction was studied to identify the optimal parameters for the primary reaction (Table 4).

Table 4- Tests conducted for optimizing the CO_2 cyclization reaction

Reaction Number	Volume of Styrene Epoxide (ml)	Amount of Catalyst (mg)	Reaction Time (h)	Reaction Temperature (ºC)	Solvent	Conversion
MIL-101-Cr	0.24	50	24	60	Methanol	10%
MIL-101-Cr	0.24	50	24	80	Methanol	27%
MIL-101-Cr	0.24	50	48	80	Methanol	70%
Defective(banzoicacid)	0.24	50	24	60	Methanol	15%
Defective(banzoic acid)	0.24	50	24	80	Methanol	93%
Defective(banzoic acid)	0.24	50	48	80	Methanol	95%

Conclusion

This study successfully synthesized defect-engineered MIL-101-Cr using benzoic acid as a modulator, enhancing its catalytic performance. XRD analysis confirmed the successful synthesis and crystallinity of both the defect-free and defective structures. SEM characterization revealed significant morphological changes, including the formation of irregular particles and surface defects, which contributed to improved catalytic activity. TGA results indicated enhanced thermal stability of the defective MOF, supporting its suitability for high-temperature applications. Catalytic tests demonstrated the impact of defect engineering. The defect-free MIL-101-Cr showed a CO_2 conversion rate of 11% at 50°C, whereas the defective MIL-101-Cr achieved a 90% conversion rate and 98% selectivity at 110°C and 1.5 bar CO_2 pressure over 24 hours. Additionally, in epoxide ring-opening reactions, the defective MOF reached a maximum conversion of 95% at 80°C using methanol. These results highlight the importance of defect engineering and morphological optimization in improving MOF functionality, establishing defective MIL-101-Cr as a highly effective catalyst for CO_2 utilization and green chemistry applications.

Conflict of interest

The authors declares that they have no conflicts of interest.

References:

[1] R. Grünker, V. Bon, P. Müller, U. Stoeck, S. Krause, U. Mueller, I. Senkovska, S. Kaskel, A new metal-organic framework with ultra-high surface area, Chem. Commun. 50 (2014) 3450–3452. https://doi.org/10.1039/c4cc00113c.

[2] C. Duan, F. Li, H. Zhang, J. Li, X. Wang, H. Xi, Template synthesis of hierarchical porous metal-organic frameworks with tunable porosity, RSC Adv. 7 (2017) 52245–52251. https://doi.org/10.1039/c7ra08798e.

[3] A.J. Howarth, Y. Liu, P. Li, Z. Li, T.C. Wang, J.T. Hupp, O.K. Farha, Chemical, thermal and mechanical stabilities of metal-organic frameworks, Nat. Rev. Mater. 1 (2016) 1–16. https://doi.org/10.1038/natrevmats.2015.18.

[4] H. Li, K. Wang, Y. Sun, C.T. Lollar, J. Li, H.C. Zhou, Recent advances in gas storage and separation using metal–organic frameworks, Mater. Today 21 (2018) 108–121. https://doi.org/10.1016/j.mattod.2017.07.006.

[5] H. Li, L. Li, R.B. Lin, W. Zhou, Z. Zhang, S. Xiang, B. Chen, Porous metal-organic frameworks for gas storage and separation: Status and challenges, EnergyChem 1 (2019) 100006. https://doi.org/10.1016/j.enchem.2019.100006.

[6] C. Chen, X. Ji, Y. Xiong, J. Jiang, Ni/Ce co-doping metal–organic framework catalysts with oxygen vacancy for catalytic transfer hydrodeoxygenation of lignin derivatives vanillin, Chem. Eng. J. 481 (2024) 148555. https://doi.org/10.1016/j.cej.2024.148555.

[7] Z. Wang, A. Bilegsaikhan, R.T. Jerozal, T.A. Pitt, P.J. Milner, Evaluating the Robustness of Metal-Organic Frameworks for Synthetic Chemistry, ACS Appl. Mater. Interfaces 13 (2021) 17517–17531. https://doi.org/10.1021/acsami.1c01329.

[8] F. Jing, R. Liang, J. Xiong, R. Chen, S. Zhang, Y. Li, L. Wu, Chromium(III) Terephthalate Metal Organic Framework (MIL-101): HF-Free Synthesis, Structure, Polyoxometalate Composites, and Catalytic Properties, Appl. Catal. B Environ. 206 (2017) 9–15.

[9] Y. Xu, X. Gao, Q. Wang, X. Wang, Z. Ji, C. Gao, Highly stable MIL-101(Cr) doped water permeable thin film nanocomposite membranes for water treatment, RSC Adv. 6 (2016) 82669–82675. https://doi.org/10.1039/c6ra16896e.

[10] H. Zhuang, W. Zhang, L. Wang, Y. Zhu, Y. Xi, X. Lin, Vapor Deposition-Prepared MIL-100(Cr)-And MIL-101(Cr)-Supported Iron Catalysts for Effectively Removing Organic Pollutants from Water, ACS Omega 6 (2021) 25311–25322. https://doi.org/10.1021/acsomega.1c03118.

[11] Z. Fang, B. Bueken, D.E. De Vos, R.A. Fischer, Defect-Engineered Metal-Organic Frameworks, Angew. Chemie - Int. Ed. 54 (2015) 7234–7254. https://doi.org/10.1002/anie.201411540.

[12] Z. Fang, J.P. Dürholt, M. Kauer, W. Zhang, C. Lochenie, B. Jee, B. Albada, N. Metzler-Nolte, A. Pöppl, B. Weber, M. Muhler, Y. Wang, R. Schmid, R.A. Fischer, Structural complexity in metal-organic frameworks: Simultaneous modification of open metal sites and hierarchical porosity by systematic doping with defective linkers, J. Am. Chem. Soc. 136 (2014) 9627–9636. https://doi.org/10.1021/ja503218j.

[13] M.A. Syzgantseva, C.P. Ireland, F.M. Ebrahim, B. Smit, O.A. Syzgantseva, Metal Substitution as the Method of Modifying Electronic Structure of Metal-Organic Frameworks, J. Am. Chem. Soc. 141 (2019) 6271–6278. https://doi.org/10.1021/jacs.8b13667.
[14] S. He, L.X. Li, L.T. Zhang, S. Zeng, C. Feng, X.X. Chen, H.L. Zhou, X.C. Huang, Elucidating influences of defects and thermal treatments on CO2 capture of a Zr-based metal–organic framework, Chem. Eng. J. 479 (2024) 147605. https://doi.org/10.1016/j.cej.2023.147605.
[15] J. Wang, L. Liu, C. Chen, X. Dong, Q. Wang, L. Alfilfil, M.R. Alalouni, K. Yao, J. Huang, D. Zhang, Y. Han, Engineering effective structural defects of metal-organic frameworks to enhance their catalytic performances, J. Mater. Chem. A 8 (2020) 4464–4472. https://doi.org/10.1039/c9ta12230c.
[16] A. Zhang, B. Liu, M. Liu, Z. Xie, D. Wang, G. Feng, The adsorption properties of defect controlled metal-organic frameworks of UiO-66, Sep. Purif. Technol. 270 (2021) 118842. https://doi.org/10.1016/j.seppur.2021.118842.
[17] K. Wang, C. Li, Y. Liang, T. Han, H. Huang, Q. Yang, D. Liu, C. Zhong, Rational construction of defects in a metal-organic framework for highly efficient adsorption and separation of dyes, Chem. Eng. J. 289 (2016) 486–493. https://doi.org/10.1016/j.cej.2016.01.019.
[18] H. Salehizadeh, N. Yan, R. Farnood, Recent advances in microbial CO2 fixation and conversion to value-added products, Chem. Eng. J. 390 (2020) 124584. https://doi.org/10.1016/j.cej.2020.124584.
[19] K. Eyuboglu, RESEARCH ARTICLE A new perspective to environmental degradation : the linkages between higher education and CO 2 emissions, (2020).
[20] P. Xu, J. Li, J. Qian, B. Wang, J. Liu, R. Xu, P. Chen, W. Zhou, Recent advances in CO2 fixation by microalgae and its potential contribution to carbon neutrality, Chemosphere 319 (2023) 137987. https://doi.org/10.1016/j.chemosphere.2023.137987.
[21] A. Nisar, S. Khan, M. Hameed, A. Nisar, H. Ahmad, S.A. Mehmood, Bio-conversion of CO2 into biofuels and other value-added chemicals via metabolic engineering, Microbiol. Res. 251 (2021) 126813. https://doi.org/10.1016/j.micres.2021.126813.
[22] Y. Yang, L. Jin, L. Zhou, X. Du, A molecular study of humid CO2 adsorption capacity by Mg-MOF-74 surfaces with ligand functionalization, Comput. Mater. Sci. 209 (2022) 111407. https://doi.org/10.1016/j.commatsci.2022.111407.
[23] K. Huang, Q. Li, X.Y. Zhang, D. Bin Qin, B. Zhao, Copper-Cluster-Based MOF as a Heterogeneous Catalyst for CO2Chemical Fixation and Azide-Alkyne Cycloaddition, Cryst. Growth Des. 22 (2022) 6531–6538. https://doi.org/10.1021/acs.cgd.2c00733.
[24] J.J. Han, Q. ruo Yan, Z. wen Chen, Z. Wang, C. Chen, Application of Cr-metal organic framework (MOF) modified polyaniline/graphene oxide materials in supercapacitors, Ionics (Kiel). 28 (2022) 2349–2362. https://doi.org/10.1007/s11581-022-04443-4.
[25] M.K. Leszczyński, K. Niepiekło, M. Terlecki, I. Justyniak, J. Lewiński, Chromium(II)-isophthalate 2D MOF with Redox-Tailorable Gas Adsorption Selectivity, ACS Appl. Mater. Interfaces 16 (2024) 45100–45106. https://doi.org/10.1021/acsami.4c06228.
[26] H. Hassan, M. Shoaib, khakemin khan, M.A. Ghanem, M. Osman, Graphene quantum dots decorated on chromium oxide and zirconium metal-organic framework composite (GQDs@Zr-MOF/Cr2O3) for asymmetric supercapacitors and hydrogen production, Mater. Chem. Phys. 332 (2025) 130225. https://doi.org/10.1016/j.matchemphys.2024.130225.
[27] C.Y. Huang, M. Song, Z.Y. Gu, H.F. Wang, X.P. Yan, Probing the adsorption characteristic of metal-organic framework MIL-101 for volatile organic compounds by quartz crystal microbalance, Environ. Sci. Technol. 45 (2011) 4490–4496. https://doi.org/10.1021/es200256q.
[28] C. Serre, F. Millange, G. Fe, A Chromium Terephthalate – Based Solid with Unusually Large Pore Volumes and Surface Area, 309 (2005).
[29] Y. Zhang, C. Sun, Y. Ji, K. Bi, H. Tian, B. Wang, Engineering linker-defects of MIL-101 series metal organic frameworks for boosted Yb (III) adsorption, Sep. Purif. Technol. 330 (2024) 125293. https://doi.org/10.1016/j.seppur.2023.125293.
[30] K. Suttiponparnit, J. Jiang, M. Sahu, S. Suvachittanont, T. Charinpanitkul, P. Biswas, Role of Surface Area, Primary Particle Size, and Crystal Phase on Titanium Dioxide Nanoparticle Dispersion Properties, Nanoscale Res. Lett. 6 (2011) 1–8. https://doi.org/10.1007/s11671-010-9772-1.
[31] J. Wang, Y. Xia, Y. Dong, R. Chen, L. Xiang, S. Komarneni, Defect-rich ZnO nanosheets of high surface area as an efficient visible-light photocatalyst, Appl. Catal. B Environ. 192 (2016) 8–16. https://doi.org/10.1016/j.apcatb.2016.03.040.

[32] C. Yang, Y. Lu, L. Zhang, Z. Kong, T. Yang, L. Tao, Y. Zou, S. Wang, Defect Engineering on CeO2-Based Catalysts for Heterogeneous Catalytic Applications, Small Struct. 2 (2021). https://doi.org/10.1002/sstr.202100058.
[33] X. Ren, C.C. Wang, Y. Li, P. Wang, S. Gao, Defective SO3H-MIL-101(Cr) for capturing different cationic metal ions: Performances and mechanisms, J. Hazard. Mater. 445 (2023). https://doi.org/10.1016/j.jhazmat.2022.130552.
[34] S. Xu, S. Chansai, C. Stere, B. Inceesungvorn, A. Goguet, K. Wangkawong, S.F.R. Taylor, N. Al-janabi, C. Hardacre, P.A. Martin, X. Fan, Sustaining metal – organic frameworks for water – gas shift catalysis by non-thermal plasma - Supplementary Information, Nat. Catal. 2 (2019) 142–148.
[35] L.J. Zhang, F.Q. Li, J.X. Ren, L.B. Ma, M.Q. Li, Preparation of metal organic frameworks MIL-101 (Cr) with acetic acid as mineralizer, IOP Conf. Ser. Earth Environ. Sci. 199 (2018). https://doi.org/10.1088/1755-1315/199/4/042038.
[36] R.A. Yang, S. Cho, S.N. Hughes, M.L. Sarazen, Implications of Defect Density and Polymer Interactions for CO2 Capture on Amine-Functionalized MIL-101(Cr), ChemSusChem 202400249 (2024) 1–13. https://doi.org/10.1002/cssc.202400249.
[37] A. Bezaatpour, M. Amiri, H. Vocke, P. Bottke, M.F. Zastrau, M. Weers, M. Wark, Low-pressure CO2fixation with epoxides via a new modified nano crystalline NH2-MIL-101(Cr) in Solvent-free and cocatalyst free condition, J. CO2 Util. 68 (2023) 102366. https://doi.org/10.1016/j.jcou.2022.102366.